# Collision Statistics of Inertial Particles in Two-Dimensional Homogeneous Isotropic Turbulence with an Inverse Cascade

**Ryo Onishi[1]†, and J. C. Vassilicos[2]**

[1]Earth Simulator Center, Japan Agency for Marine-Earth Science and Technology, 3173-25 Showa-machi, Kanazawa-ku Yokohama Kanagawa, 236-0001, Japan

[2]Department of Aeronautics, Imperial College London, SW7 2AZ, UK

(Received ?; revised ?; accepted ?. - To be entered by editorial office)

This study investigates the collision statistics of inertial particles in inverse-cascading two-dimensional (2D) homogeneous isotropic turbulence by means of a direct numerical simulation (DNS). A collision kernel model for small Stokes number ($St$) particles in 2D flows is proposed based on the model of Saffman & Turner (1956) (ST56 model). The DNS results agree with this 2D version of the ST56 model for $St \lesssim 0.1$. It is then confirmed that our DNS results satisfy the 2D version of the spherical formulation of the collision kernel. The fact that the flatness factor stays around three in our 2D flow confirms that the present 2D turbulent flow is nearly intermittency free. Collision statistics for $St$=0.1, 0.4 and 0.6, i.e., for $St$<1, are obtained from the present 2D DNS and compared with those obtained from the 3D DNS of Onishi *et al.* (2013). We have observed that the 3D radial distribution function at contact ($g(R)$, the so-called clustering effect) decreases for $St$=0.4 and 0.6 with increasing Reynolds number, while the 2D $g(R)$ do not show a significant Reynolds number dependence. This observation supports the view that the Reynolds number dependence of $g(R)$ observed in 3D is due to internal intermittency of the 3D turbulence. We have further investigated the local $St$, which is a function of the local flow strain rates, and proposed a plausible mechanism that can explain the Reynolds number dependence of $g(R)$. Meanwhile, 2D stochastic simulations based on the Smoluchowski equations for $St \ll 1$ show that the collision growth can be predicted by the 2D ST56 model and that rare but strong events do not play a significant role in such a small-$St$ particle system. However, the PDF of local $St$ at the sites of colliding particle pairs supports the view that powerful rare events can be important for particle growth even in the absence of internal intermittency when $St$ is not much smaller than unity.

## 1. Introduction

Several mechanisms have been proposed in the literature to explain what causes the fast size-broadening of cloud droplets, which could result in quick rain initiation at the early stage of cloud development. Examples are enhanced collision rates of cloud droplets by turbulence (Falkovich & Pumir 2007; Grabowski & Wang 2009, 2013), turbulent entrainment (Blyth 1993; Krueger *et al.* 1997), giant cloud condensate nuclei (Yin *et al.* 2000; Van Den Heever & Cotton 2007) and turbulent dispersions of condensing cloud droplets (Sidin *et al.* 2009). The most intensely discussed is the first mechanism; enhanced collision rate by turbulence. This has initiated extensive research on particle collisions in

† Email address for correspondence: onishi.ryo@jamstec.go.jp

turbulence (Sundaram & Collins 1997; Wang *et al.* 2000; Saw *et al.* 2008; Onishi *et al.* 2009; Dallas & Vassilicos 2011, and references therein).

There are several collision models that predict collision rates of particles in turbulence. Saffman & Turner (1956) analytically derived a collision model for particles with zero or very small Stokes number, $St$ ($=\tau_p/\tau_\eta$, where $\tau_p$ is the particle relaxation time and $\tau_\eta$ the Kolmogorov time), while Abrahamson (1975) derived a model for particles with much larger $\tau_p$ than $T_I$, the integral time scale of the turbulence. Water droplets typically have $St = O(10^{-2\sim0})$ and $St = O(10^{0\sim2})$ when they are rain droplets. One difficulty arises from the preferential motion of inertial particles. Inertial particles preferentially cluster and accumulate in regions of low vorticity and high strain if $St < 1$ (Maxey 1987; Chun *et al.* 2005), and cluster in a way to mimic the clustering of zero-acceleration points by the sweep-stick mechanism if $1 \lesssim St \lesssim \tau_p/T_I$ (Coleman & Vassilicos 2009). This matters because clustering increases the mean collision rate (Sundaram & Collins 1997). The clustering effect makes the construction of a fully-analytical model for finite-inertial particles very difficult, and requires several empirical parameters in collision models (Zhou *et al.* 2001; Wang *et al.* 2000; Zaichik *et al.* 2003; Onishi 2005; Franklin *et al.* 2007). Those parameters are usually determined by direct numerical simulation (DNS) data. Data from laboratory experiments (Saw *et al.* 2008; Lu *et al.* 2010; Bordas *et al.* 2011) would of course help, but available data are very much limited.

One serious problem is that the Reynolds number dependence of turbulent collisions has not been clarified yet. The Taylor-microscale based Reynolds number $R_\lambda$ ($= u' l_\lambda/\nu$, where $u'$ is the rms of velocity fluctuations, $l_\lambda$ the Taylor microscale and $\nu$ the kinematic viscosity) for collision statistics attained by DNS is $R_\lambda = O(10^2)$. This value is much smaller than those in cloud turbulence, where $R_\lambda$ ranges from $10^3$ up to nearly $10^5$ (It is often estimated as $R_\lambda$ of $10^{3-4}$ in literature. However, $R_\lambda$ is estimated up to 5-8$\times10^4$ in MacPherson & Isaac (1977), and Siebert *et al.* (2006) observed $R_\lambda$ of 3-4$\times10^4$.). Nevertheless, there are several studies where collision models are used in cloud simulations to investigate the impact of enhanced collisions of cloud droplets (Onishi *et al.* 2006; Xue *et al.* 2008; Wang *et al.* 2009; Onishi *et al.* 2011). These studies simply extrapolate their collision models to high $R_\lambda$, without justification. A simple solution would be to obtain collision statistics for high $R_\lambda$ flows, which requires high-performance computing.

Onishi *et al.* (2013) recently extended the upper limit in $R_\lambda$ by DNS. They attained $R_\lambda$=530 and reported a dependence of collision statistics on Reynolds number for $R_\lambda$>100. They observed that the clustering effect, and consequently the collision kernel, decreases as $R_\lambda$ increases for $R_\lambda$>100 and $St$=0.4, while no significant Reynolds number dependence was observed for $St$=0.1. This is a relevant and significant observation since many authors ignore this Reynolds number dependence and assume a constant collision kernel irrespective of $R_\lambda$ (Saffman & Turner 1956; Derevyanko *et al.* 2008; Zaichik & Alipchenkov 2009) or assume a convergence to a constant collision kernel with increasing $R_\lambda$ (Ayala *et al.* 2008). A similar Reynolds number dependence for $St < 1$ has now been confirmed by Rosa *et al.* (2013). Onishi *et al.* (2013) anticipated that this Reynolds number dependence might be due to the intermittent nature of high Reynolds number turbulence. However, no evidence for this has been obtained so far.

The present study, therefore, aims to obtain evidence that the intermittent nature of small-scale turbulence influences the collision statistics, leading to this Reynolds number dependence. To achieve this goal, the present study utilizes two-dimensional (2D) isotropic turbulence with inverse cascade because such turbulent flows have little internal intermittency (Tabeling 2002) thus allowing an assessment of the significance of intermittency by comparing 2D and 3D DNS turbulence results. We therefore develop a DNS for colliding inertial droplets in 2D isotropic turbulence with inverse cascade; the

code is composed of the flow code by Goto & Vassilicos (2004), the particle code by Dallas & Vassilicos (2011) and the collision statistics code by Onishi *et al.* (2009). Then we compare the present results with the 3D results of Onishi *et al.* (2013).

In order to investigate the role of intermittency, the present study employs intermittency-free inverse-cascading 2D turbulence as a counterpart for comparisons with 3D turbulence where intermittency is strong. Another option would have been to employ a synthetic flow simulation, such as a phase-shuffled simulation (Yoshimatsu *et al.* 2009) or a kinematic simulation (Chen *et al.* (2006); Goto *et al.* (2005) and references therein). The phase-shuffled flow can be obtained by decomposing the DNS velocity field into Fourier modes and randomizing the phases of the coefficients. This method preserves energy, but breaks the flow structure and makes the flow intermittency-free. The phase-shuffled flow has a full set of flow modes, while the kinematic flow has only a fraction of modes. Both flows can mimic the -5/3 power-law energy spectrum and both have intermittency-free, i.e. Gaussian, statistics of fluctuating velocity difference. Yoshimatsu *et al.* (2009) reported that phase-shuffled turbulence does not preserve the acceleration's scaling behavior which implies that the acceleration physics, which are of central importance in particle clustering and collisions, are different from Navier-Stokes turbulence. Chen *et al.* (2006) reported that in kinematic simulations of turbulence, particle clustering results from the repelling action of velocity stagnation-point clusters, a clustering mechanism which is very different from those in Navier-Stokes turbulence. These facts suggest that synthetic simulations of turbulence are not the best option for a comparative discussion of the effect of intermittency on particle clustering and resulting Reynolds number dependencies. This is why we chose DNS of inverse-cascading 2D turbulence for this purpose.

In the following section, we briefly introduce theoretical results for turbulent collision statistics including the presently-derived 2D theoretical results. Our 2D DNS code is presented in section 3. Numerical results and discussion are presented in section 4, which consists of flow statistics in subsection 4.1 and mostly particle statistics in subsection 4.2. We conclude in section 5.

## 2. Collision Statistics Theories

### 2.1. *Collision kernel for small Stokes particles*

The Stokes number is defined as

$$St = \frac{\tau_p}{\tau_\eta}, \tag{2.1}$$

where $\tau_p$ $(= 2\rho_p r^2/(9\rho_a \nu))$, where $r$ is the droplet radius and $\rho_p/\rho_a$ the ratio of the density of the liquid water to that of air) is the particle relaxation time, and $\tau_\eta (=\sqrt{\nu/\epsilon}$, where $\nu$ is the kinematic viscosity and $\epsilon$ the energy dissipation rate) the Kolmogorov time. $St$ is the non-dimensional parameter of particle inertia and $St = 0$ corresponds to means a tracer particle, which follows the carrier flow perfectly.

The collision rate per unit area and time between a particle of radius $r_1$ and a particle of radius $r_2$ is given by

$$N_c(r_1, r_2) = K_c(r_1, r_2) n_{p1} n_{p2}, \tag{2.2}$$

where $K_c$ is the collision kernel and $n_{p1}$ and $n_{p2}$ are droplet number concentrations. Saffman & Turner (1956) derived the collision kernel for $St \ll 1$ in three-dimensional

(3D) isotropic turbulence as

$$\langle K_c(r_1,r_2)\rangle_{\mathrm{ST,3D}} = \sqrt{2\pi}R^2\left[\left(1-\frac{\rho_a}{\rho_p}\right)^2(\tau_{p1}-\tau_{p2})^2\overline{\left(\frac{Du}{Dt}\right)^2}\right.$$
$$\left.+\frac{1}{3}\left(1-\frac{\rho_a}{\rho_p}\right)^2(\tau_{p1}-\tau_{p2})^2 g^2+\frac{1}{15}\lambda^2R^2\right]^{1/2} \tag{2.3}$$

where $\langle\cdots\rangle$ denotes an ensemble average, $r_1$ and $r_2$ are the radii of each particle respectively, $\lambda = 1/\tau_\eta$, $g$ is the gravitational acceleration and $R = r_1 + r_2$ is the collision radius. Neglecting gravity and using $\rho_a/\rho_p \ll 1$, the above equation reads

$$\langle K_c(r_1,r_2)\rangle_{\mathrm{ST,3D}} = \sqrt{2\pi}R^2\left[(\tau_{p1}-\tau_{p2})^2\overline{\left(\frac{Du}{Dt}\right)^2}+\frac{1}{15}\lambda^2R^2\right]^{1/2}. \tag{2.4}$$

The first term in the square bracket is the acceleration contribution, and the second the shear contribution. When $r_1 = r_2$, i.e., for the monodisperse case, the acceleration contribution disappears because $\tau_{p1} = \tau_{p2}$ and we obtain

$$\langle K_c(r_1,r_1)\rangle_{\mathrm{ST,3D}} = \sqrt{\frac{2\pi}{15}}\lambda R^3. \tag{2.5}$$

The 15 in the square-root originates from the relation $\epsilon/\nu = 15\left\langle(\partial u/\partial x)^2\right\rangle$ for three-dimensional isotropic turbulence (Taylor 1935). Two dimensionality reduces the freedom in dimension, leading to $\epsilon/\nu = 8\left\langle(\partial u/\partial x)^2\right\rangle$. This leads to collision kernels for bidisperse droplets and monodisperse droplets with $St \ll 1$ in two-dimensional isotropic turbulence as

$$\langle K_c(r_1,r_2)\rangle_{\mathrm{ST,2D}} = \sqrt{2\pi}R\left[(\tau_{p1}-\tau_{p2})^2\overline{\left(\frac{Du}{Dt}\right)^2}+\frac{1}{8}\lambda^2R^2\right]^{1/2} \tag{2.6}$$

and

$$\langle K_c(r_1,r_1)\rangle_{\mathrm{ST,2D}} = \frac{\sqrt{\pi}}{2}\lambda R^2, \tag{2.7}$$

respectively.

### 2.2. *The spherical formulation*

Wang *et al.* (1998*b*) formulated the collision kernel in three-dimensional flows based on the spherical formulation as

$$\langle K_c(r_1,r_2)\rangle_{\mathrm{3D}} = 2\pi R^2\langle|w_r(x=R)|\rangle\, g(x=R), \tag{2.8}$$

where $w_r(x=R)$ ($w_r$ hereafter) is the radial relative velocity at contact, and $g(x=R)$ ($g(R)$ hereafter) the radial distribution function, RDF, at contact. The RDF $g(R)$ represents the clustering effect and is equal to unity when particles are uniformly distributed. One important assumption behind Eq. (2.8) is that the relative velocity is incompressible, thus influx and outflux across the sphere surface are equal. The collision kernel is then half the surface area multiplied by the average magnitude of the radial relative velocity and by $g(R)$.

Based on the same assumption, the two-dimensional version of the spherical formulation can be derived as

$$\langle K_c(r_1, r_2)\rangle_{2\mathrm{D}} = \pi R \langle |w_r| \rangle g(R). \tag{2.9}$$

## 3. Two-dimensional Direct Numerical Simulation

### 3.1. *Flow simulation*

The code developed by Goto & Vassilicos (2004) was used to generate a two-dimensional statistically-stationary homogeneous isotropic turbulent flow in a periodic box of length $2\pi$ with an inverse energy cascade giving rise to an energy spectrum $\propto k^{-5/3}$. The DNS scheme integrates in time the modified vorticity ($\boldsymbol{\omega}$) equation,

$$\frac{\partial \boldsymbol{\omega}}{\partial t} = \nabla \times (\mathbf{u} \times \boldsymbol{\omega}) + \hat{D}\boldsymbol{\omega} + \mathbf{f}, \tag{3.1}$$

in wave number space using a fourth-order Runge-Kutta scheme, with the nonlinear term calculated in real space, i.e., a pseudo-spectral method is adopted. $\mathbf{u}$ is the fluid velocity and $\mathbf{f}$ is the external forcing to maintain a statistically-stationary state. The forcing acts only on the Fourier components in the wavenumber range between $k_f$ and $\beta k_f$ ($\beta$ is a constant, slightly larger than 1). The dissipation operator $\hat{D}$ is defined as

$$\hat{D} = \left[-\nu\Delta^8 + \alpha\Delta^{-1}\right], \tag{3.2}$$

and allows for large-scale dissipation in 2D flows through hyperdrag ($\alpha$ term). The high (specifically 8)-order hyper-viscosity ensures that the small-scale enstrophy dissipation does not contaminate inertial-range statistics. This choice (3.2) of dissipation operator produces a well-defined $k^{-5/3}$ energy spectrum. More details on this two-dimensional turbulence simulation can be found in Goto & Vassilicos (2004) and Faber & Vassilicos (2010).

The numerical choices for the 2D flows are summarized in Table 1. In order to prevent the forcing from directly affecting particle motions, wave motions with $k > k_c$, where $k_c = k_f/1.2$ (Dallas & Vassilicos 2011), were filtered out from the fluid velocity field used to calculate particle trajectories and statistics as well as related flow statistics. In order to compare the present 2D results with the 3D results of Onishi *et al.* (2013), we introduce the following Reynolds number

$$Re_T = \frac{T_I}{\tau_\eta}, \tag{3.3}$$

where $T_I$ is the integral time ($= L_I/u'$, where $u'$ is the rms of fluctuating velocity and $L_I (= \pi/2u'^2 \int_0^\infty E(k)k^{-1}dk$, where $E(k)$ is the energy spectrum) the integral length) and $\tau_\eta$ is calculated as $\tau_\eta = 1/\sqrt{2\langle tr(\mathbf{s}^2)\rangle}$, where $\mathbf{s}$ is the strain rate tensor, whose components $s_{ij} = (\partial_i u_j + \partial_j u_i)/2$ are obtained after low-pass filtering at $k = k_c$. This $Re_T$ is proportional to $(L_I/\eta)^{2/3}$, where $\eta \left(= (\nu^3/\epsilon)^{1/4}\right)$ is the Kolmogorov scale, for the 3D homogeneous isotropic turbulence and to $(L_I/l_c)^{2/3}$, where $l_c = 2\pi/k_c$, for the 2D one.

### 3.2. *Particle simulation*

Water droplets are considered as Stokes particles with inertia governed by the equation

| Run | $N^2$ | $k_f$ | $\beta$ | $\nu$ | $L_I$ | $u'$ | $Re_T$ |
|---|---|---|---|---|---|---|---|
| N64 | $64^2$ | 13 | 1.08 | $9.0 \times 10^{-19}$ | 0.696 | 6.12 | 6.12 |
| N128 | $128^2$ | 26 | 1.04 | $2.5 \times 10^{-23}$ | 0.606 | 5.20 | 8.32 |
| N256 | $256^2$ | 51 | 1.02 | $8.0 \times 10^{-28}$ | 0.536 | 4.35 | 11.3 |
| N512 | $512^2$ | 102 | 1.01 | $2.5 \times 10^{-32}$ | 0.467 | 3.38 | 16.4 |
| N1024 | $1024^2$ | 205 | 1.005 | $7.5 \times 10^{-37}$ | 0.406 | 2.55 | 23.4 |
| N2048 | $2048^2$ | 410 | 1.0025 | $2.0 \times 10^{-41}$ | 0.355 | 2.13 | 30.5 |
| N4096 | $4096^2$ | 819 | 1.00125 | $6.0 \times 10^{-46}$ | 0.281 | 1.35 | 41.1 |

TABLE 1. Parameters for the two-dimensional isotropic turbulence with inverse cascade.

$$\frac{d\mathbf{v}(\mathbf{x_p})}{dt} = -\frac{1}{\tau_p}\left(\mathbf{v}(\mathbf{x_p}) - \mathbf{u}(\mathbf{x_p})\right) \tag{3.4}$$

where $\mathbf{v}$ is the particle velocity and $\mathbf{x_p}$ the particle position. Onishi *et al.* (2009) showed that gravity is not a relevant factor for collisions of monodisperse small water droplets in a 3D homogeneous isotropic turbulence and Onishi *et al.* (2013) simply neglected gravity. For the sake of comparisons with Onishi *et al.* (2013), this study also neglects gravity. The fourth-order Runge-Kutta method was used for time integration of particle positions and velocities. The flow velocity at a particle position was interpolated using fifth-order Lagrangian interpolation. Turbulence modulation by droplets was assumed negligible because of high particle dilution.

There are several ways to deal with collision events. One of the colliding droplets may be removed immediately after collision (*Scheme 1*), or droplets may be allowed to overlap (ghost-particle condition) (*Scheme 2*). Scheme 1 is more realistic because the collision-coalesced droplet will form a particle of larger size and will disappear from the original size group. Scheme 2 is suitable for discussing the so-called spherical form (refer to Eqs. (2.8) and (2.9)), where the effect of clustering is clear. In order to include a discussion of the clustering effect this study employs Scheme 2.

After the 2D background airflow reached a statistically-stationary state, water droplets were introduced into the flow. Collision detection was then started after a period exceeding thirty times the integral time $T_I$. The collision rate between particles $r_1$ and particles $r_2$ at the $n$-th timestep $N_c^n(r_1, r_2)$ is calculated from the number of collision pairs $N_{col.pair}^n(r_1, r_2)$ detected in the domain for a time interval $\Delta t$ as $N_c^n = N_{col.pair}^n/(S_d \Delta t)$, where $S_d$ is the area of the computational domain. Thus, the collision kernel at the $n$-th time step, $K_c^n$, is obtained as

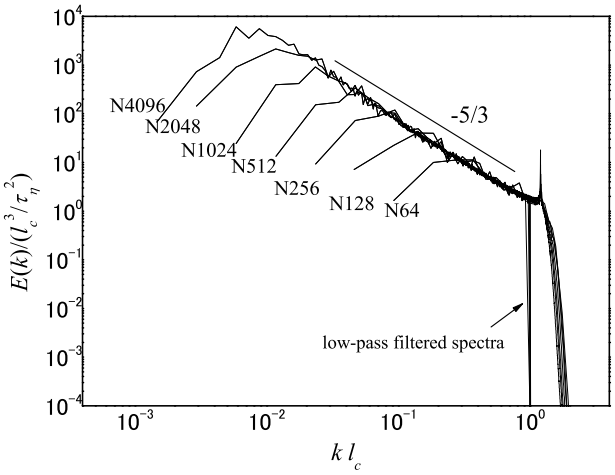


FIGURE 1. Energy spectra of the present 2D flow.

$$K_c^n(r_1, r_2) = \frac{N_{col.pair}^n(r_1, r_2)}{n_{p1} n_{p2} S_d \Delta t}, \tag{3.5}$$

where $n_{pi} = N_{pi}/S_d$, where $N_{pi}$ ($i$=1,2) is the total number of particles with radius $r_i$ and $S_d = (2\pi)^2$. The mean collision kernel, $\langle K_c \rangle$, is calculated by time averaging the collision kernels over the duration of the collision simulation. The radial relative velocity at contact $\langle |w_r| \rangle$, and the RDF at contact $g(R)$ are calculated based on the algorithm of Wang *et al.* (2000). A method based on molecular-dynamic-simulation strategies was employed for detecting neighboring pairs (Sundaram & Collins 1996; Allen & Tildesley 1987).

## 4. Results and Discussion

### 4.1. *Flow statistics*

Figure 1 shows energy spectra for all the runs listed in Table 1. As Goto & Vassilicos (2004) reported, the constancy of the energy flux is achieved in the inertial range, leading to a -5/3 power law. A vertical needle shape is observed at the forcing scale, i.e., at $kl_c = 1.2$; it is filtered out by the low-pass filter at $k = k_c$.

Figure 2 shows the flatness factor defined as

$$F = \frac{\left\langle (\partial u_1/\partial x_1)^4 \right\rangle}{\left\langle (\partial u_1/\partial x_1)^2 \right\rangle^2}. \tag{4.1}$$

The flatness factor for the 3D flow increases as $Re_T$ increases, while that for the present 2D flow stays around 3 and is at most 4, which suggests a near-Gaussian distribution for $\partial u_1/\partial x_1$. This confirms that the 3D turbulence becomes more intermittent with increasing Reynolds number, while the 2D turbulence does not (to be fully accurate, its flatness factor systematically increases but the rate is much less than that of 3D turbulence)

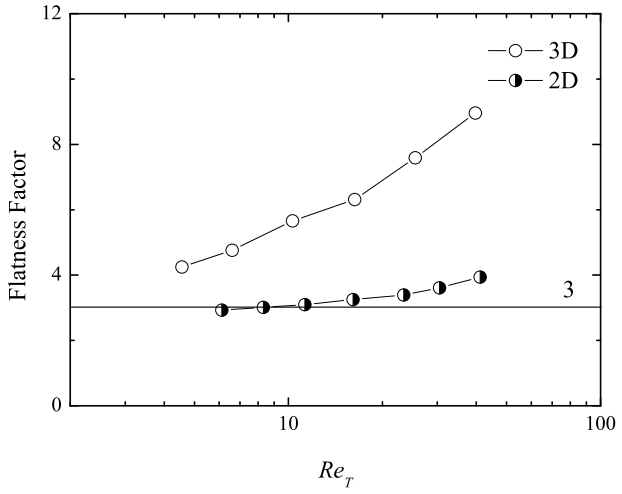


FIGURE 2. Flatness factor against $Re_T$.

(Tabeling 2002). The skewness $S$, defined as $S = \left\langle (\partial u_1/\partial x_1)^3 \right\rangle / \left\langle (\partial u_1/\partial x_1)^2 \right\rangle^{3/2}$, was also investigated and confirmed to be $O(10^{-2})$ for all the runs in the present 2D flow (not shown).

### 4.2. *Collision statistics*

#### 4.2.1. *Spherical formulation*

The radial relative velocity at contact, $\langle |w_r| \rangle$, and the RDF at contact, $g(R)$, are calculated following the algorithm by Wang *et al.* (2000), where pairs with interparticle distance $d$ such that $R - \delta/2 < d \leqslant R + \delta/2$ are considered as contacting pairs. Wang *et al.* (2000) investigated the $\delta$ dependence of $\langle |w_r| \rangle$ and $g(R)$, and observed that the two statistics are insensitive to $\delta$ if $\delta/R < 0.2$. They investigated this dependence for 3D homogeneous isotropic turbulence but no study has investigated it for a 2D flow yet.

Figure 3 shows the dependence of $\langle |w_r| \rangle$ and $g(R)$ on $\delta$ for the N256 run. The error bars were obtained from more than 5 runs, each run lasting for a time $33T_I$. $\langle |w_r| \rangle$ increases with increasing $\delta$ because slightly larger sizes of eddies of larger velocity fluctuations will contribute to the relative velocity. On the other hand, $g(R)$ decreases with increasing $\delta$ because the level of preferential concentration is reduced by a larger shell volume. It is also observed that $\langle |w_r| \rangle$ and $g(R)$ are insensitive to $\delta$ for $\delta/R < 0.2$. These observations agree well with Wang *et al.* (2000). Following Wang *et al.* (2000), this study adopts $\delta = 0.02R$ from here onwards.

The collision kernels directly obtained from Eq. (3.5) using our DNS were compared with the collision kernels obtained from Eq. (2.9) and found to deviate by 0.8% for $St$=0.4, consistent with the errors of nearly 1% previously reported in 3D DNS of homogeneous isotropic turbulence (Wang *et al.* 1998*a*; Onishi *et al.* 2013)

#### 4.2.2. *St dependence of collision statistics*

Figures 4 and 5 show the Stokes number dependence of collision statistics for the N2048 run, where the flow contained 1,024,000 particles in total. Figure 4(a) shows the

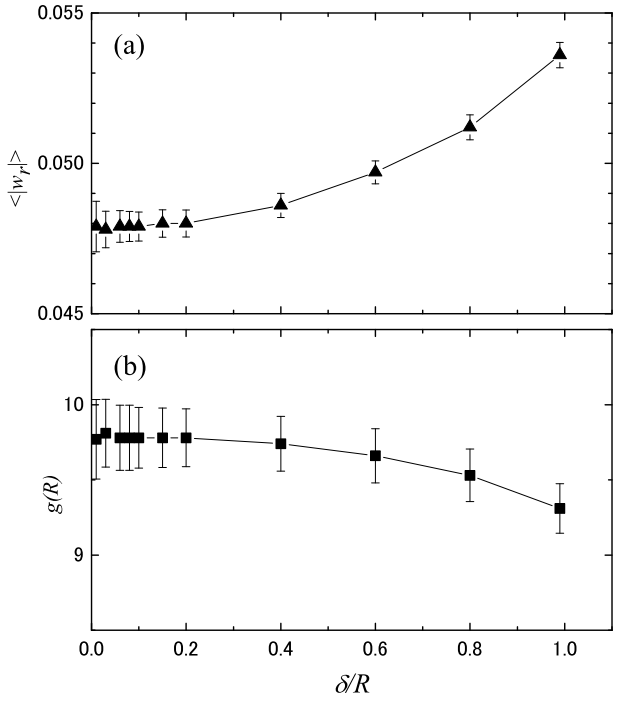


FIGURE 3. Dependence of (a) the radial relative velocity at contact, $\langle|w_r|\rangle$, and (b) the radial distribution function at contact, $g(R)$, on the thickness of the spherical shell, $\delta$.

collision kernel normalized by $\lambda R^2$. The collision kernels for small inertial particles where $St \leqslant 0.04$ are in good agreement with Eq. (2.7), while those for larger inertial particles are significantly larger than Eq. (2.7) due to their inertia. This tendency is very similar to that observed in 3D flows (e.g., Wang *et al.* (2000)). Figure 4(b) shows the residual RDF defined as $g(R)-1$. For $St \ll 1$, an analytical solution predicts that $g(R)-1 \propto St^2$ (Wang *et al.* 2000). This holds for $St \leqslant 0.04$ in the figure. Figure 4(c) shows the radial relative velocity at contact normalized by $\lambda R$. From Eqs. (2.7) and (2.9) and assuming $g(R) \sim 1$, we obtain $\langle|w_r|\rangle / \lambda R = 1/2\sqrt{\pi} = 0.282$. The 2D DNS results agree with the line of 0.282 for $St \leqslant 0.1$.

Figure 5 shows the Stokes number dependence of calculated collision kernels for bidisperse droplets. The same number of different-size droplets were introduced into the fully developed 2D isotropic turbulence for calculating the collision kernel. The Stokes number of one group of droplets was fixed at $St_1 = 0.04$, whereas that of the other group was varied between $St_2 = 0.04$ and $St_2 = 1$. The vertical axis in Figure 5 is the collision kernel $K_c(St_1 = 0.04, St_2)$ normalized by $\lambda R^2$. The present 2D DNS results agree with Eq. (2.6) for $St_2 \leqslant 0.2$ but not with Eq. (2.7) except for the case where $St_1 = St_2$. This confirms that the acceleration contribution is important if not dominant when collisions are between different-size droplets.

All the figures in this subsection have shown that the present 2D DNS results agree with theoretical predictions for $St \ll 1$, in fact, roughly speaking, for $St < 0.1$. This confirms the reliability of the present code and statistical procedures used in this study.

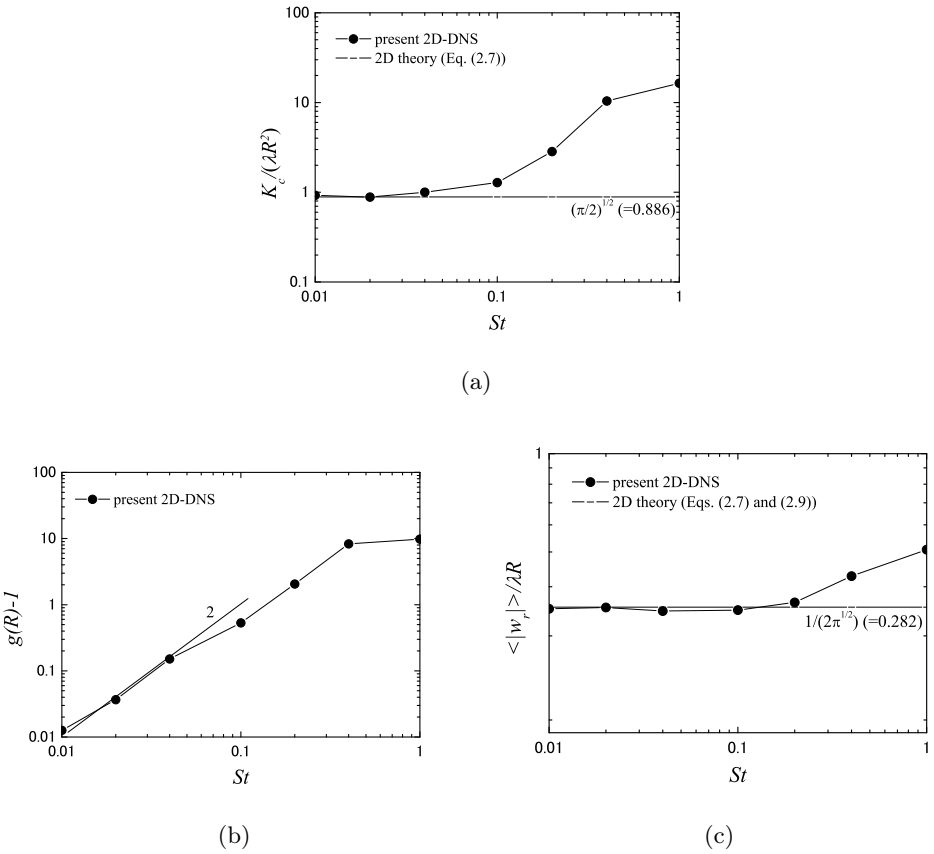


FIGURE 4. Stokes number dependency of collision statistics of monodisperse droplets in the two-dimensional isotropic turbulence.

4.2.3. *Collision growth of small inertial particles*

Dallas & Vassilicos (2011) showed a rapid growth of particles with initially very small inertia, specifically $St = 0.04$, in DNS of 2D homogeneous isotropic turbulence with -5/3 energy spectrum. They concluded that powerful rare events had lead to the rapid growth in their system. However, what we have observed so far in this study is that collision frequencies for such small inertial particles in such flows follow the Saffman and Turner theory. This subsection aims to clarify whether such powerful rare events do indeed violate the stochastic framework (consistent with the Saffman and Turner theory) at very small Stokes numbers. We perform two kinds of collision growth simulations: one is based on a stochastic (kinematic) framework, which requires collision kernels as inputs, and the other on Lagrangian integration obtained from our DNS framework. We then compare results to check whether the collision growth in the Lagrangian framework can be predicted by the stochastic framework.

Let us suppose that initially we have monodisperse droplets of type 1. Larger droplets will form by multiple collisions, and we denote by $n_s$ the number concentration of droplets with $s$ times the mass of a type 1 droplet. The radius of type $i$ droplets is $r_i = i^{1/3} r_1$, consequently its Stokes number is $St_i = i^{2/3} St_1$. We also assume that when two droplets collide they coalesce without bouncing nor breaking up. Then the following equation

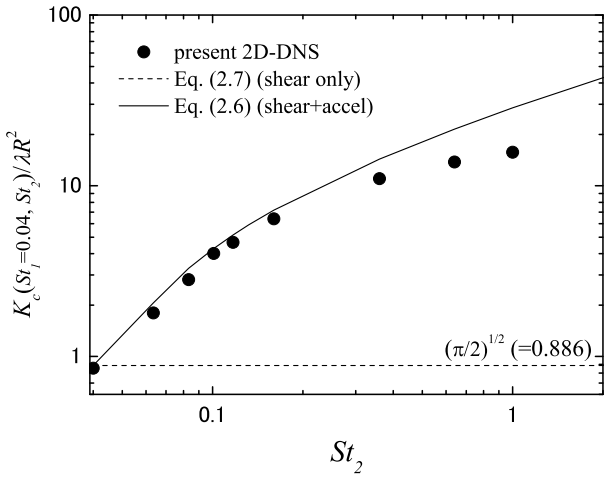


FIGURE 5. Stokes number dependency of collision statistics of bidisperse droplets in the two-dimensional isotropic turbulence. The horizontal axis shows $St_2$, while $St_1$ was fixed at 0.04.

holds (called Smoluchowski equation or stochastic collision equation)

$$\frac{dn_i}{dt} = \sum_{l+m=i} K^{\#}_{lm} n_l n_m - \sum_{j=1}^{\infty} K_{ij} n_i n_j, \tag{4.2}$$

where $K_{lm} = K_c(r_l, r_m)$ and $K^{\#}_{lm}$ is $\frac{1}{2}K_{lm}$ for $l = m$ and $K_{lm}$ otherwise. Table 2 shows the collision kernels $K^{\#}_{lm}$ for bidisperse systems obtained from our 2D DNS as described in subsection 3.2. Two more ways of calculating $K^{\#}_{lm}$ are considered in this study; Eq. (2.6) (i.e., shear+acceleration terms) and Eq. (2.7) (i.e., shear term only).

Following Dallas & Vassilicos (2011), we calculated the collision growth of droplets from a Lagrangian procedure applied to our DNS of 2D turbulence. The computational settings were basically the same as those of Dallas & Vassilicos (2011), with $2048^2$ grid points and $1.5\times10^6$ droplets. The one single difference was that the initial droplet size distribution was purely monodisperse in this study while it had small deviations in Dallas & Vassilicos (2011). We checked that the small deviations have little influence.

Figure 6 shows distributions of droplet sizes at $t/T_I = 9.5$. There were initially only $s$=1 particles, and, as the collision growth proceeds, larger $s$ particles were created. As the initial number of droplets was $1.5\times10^6 \sim \mathrm{O}(10^6)$ for the Lagrangian DNS, there is no possibility for $n_s/n_{\mathrm{ini}}$ (where $n_{\mathrm{ini}}$ is the initial number concentration) to drop below $10^{-6}$ in the present Lagrangian DNS result. However the calculations based on the stochastic equation (4.2) give values of $n_s/n_{\mathrm{ini}}$ smaller than $10^{-6}$ as indeed seen in the figure. It is clear from Figure 6 that the stochastic result with the collision kernel of Eq. (2.7) underestimates the growth speed while the result with the collision kernel of Eq. (2.6) slightly overestimates it. This observation corresponds to what we observed in Figure 5 (which showed an underestimate by Eq. (2.7) in the collision kernels and an overestimate by Eq. (2.6)) and also confirms the relevance of the acceleration term in Eq. (2.6). The stochastic result with the collision kernels pre-calculated from DNS (see Table 2) agrees

| | type $i$=1 | 2 | 3 | 4 | 5 |
|---|---|---|---|---|---|
| type $j$=1 | 0.821 | 1.73 | 2.70 | 3.87 | 4.50 |
| 2 | - | 0.938 | 1.51 | 2.38 | 3.01 |
| 3 | - | - | 1.06 | 1.51 | 3.16 |
| 4 | - | - | - | 1.20 | 1.51 |
| 5 | - | - | - | - | 1.29 |

TABLE 2. Normalized turbulent collision kernels for bidisperse particles, $K_c(i,j)/\lambda R^2$, from N2048.

with the Lagrangian DNS result. This indicates two relevant points: one is that the Lagrangian DNS and the stochastic simulations are both reliable. The other is that the stochastic approach, without considering a special treatment for powerful rare events, can predict the collision growth in this turbulence. This shows that the rapid collision growth observed in Dallas & Vassilicos (2011) can be explained by the classical stochastic framework. It should be noted, however, that Dallas & Vassilicos (2011) focused on the droplets in atmospheric clouds and adopted a system of small-inertial particles with a dilute volume fraction. The mechanism they proposed may nevertheless be valid for larger $St$ particles and/or with more dense volume fractions. This will be partly discussed in subsection 4.2.6.

4.2.4. *Reynolds number dependence of collision statistics*

Figure 7(a) shows the mean collision kernel obtained for $St$=0.4 from the present 2D DNS together with that from the 3D DNS of Onishi *et al.* (2013). The 3D DNS was performed for the flow with $R_\lambda$ ranging from 49 to 527. The largest simulation, i.e., $R_\lambda = 527$ simulation, was performed using $2{,}000^3$ grid points and one billion particles. Please refer to Onishi *et al.* (2013) for more details on the numerical schemes and procedures of the 3D DNS. The collision kernels are normalized by $\lambda R^2$ and $\lambda R^3$ for the 2D and 3D results, respectively. The error bars show ±one standard deviation. The standard deviation for 2D was obtained from more than three runs with each run lasting for a time ranging from $5T_I$ to $8T_I$ except for the N64 runs ($Re_T = 6.1$) where the time duration was $44T_I$. The particle size, $r$, was $0.00525l_c$ meaning that $r$ was much smaller than the cut-off filter scale. The total number of particles, $N_p$, was larger for larger grid number simulations so as to maintain the area fraction $\phi_A \left(= \pi r^2 N_p/(2\pi)^2\right)$ constant. $N_p$ was 1,000 for N64 and up to 4,096,000 for N4096. The area fraction $\phi_A$ was $3.78\times10^{-3}$, which corresponds to a high dilution thereby suggesting only binary collisions. The normalized collision kernel from the 3D DNS decreases for $Re_T > 7$ (corresponding to $R_\lambda$>100) as noted by Onishi *et al.* (2013). In contrast, that from the present 2D DNS does not decrease in the Reynolds range $10 < Re_T < 40$.

Figures 7(b) and (c) show the RDF and radial relative velocity at contact, i.e., $g(R)$ and $\langle|w_r|\rangle$, respectively. In the present 2D DNS, $g(R)$ decreases with increasing Reynolds number at low values of $Re_T$ but then becomes constant for $Re_T > 16$. By contrast, the 3D $g(R)$ increases at low values of $Re_T$ but then decreases for $Re_T > 7$. Furthermore, the 3D data of Onishi *et al.* (2013) in Figure 7 shows, as indeed concluded by Onishi *et al.* (2013), that the Reynolds number dependence of the collision kernel reflects, in 3D, the Reynolds number dependence of $g(R)$. Indeed as seen in Figure 7, the 3D $g(R)$ shows a similar Reynolds number dependence to the 3D collision kernel whereas the 3D $\langle|w_r|\rangle$

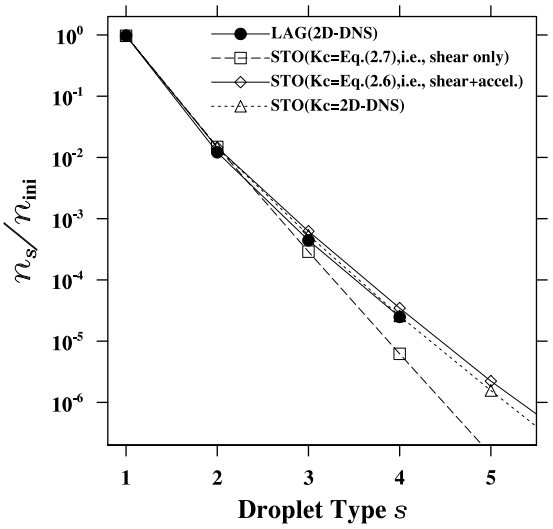


FIGURE 6. Distribution of droplet sizes produced from an initially uniform population at $t/\tau_L = 9.5$. LAG(2D-DNS) refers to the result obtained from a Lagrangian procedure applied to our 2D DNS, STO(Kc=Eq.(2.7), i.e. shear only) , STO($K_c$=Eq.(2.6), i.e., shear+accel.) and STO($K_c$=2D-DNS) refer to results obtained by solving the stochastic equation (4.2) with three different ways of obtaining collision kernels.

does not. (Note, however, that the 3D $\langle|w_r|\rangle$ slowly increases towards what appears to be a constant value and this weak trend cancels some of the decreasing trend of the 3D $g(R)$ causing the collision kernel to decrease with increasing $Re_T$ at a slightly slower rate than $g(R)$.) In 2D, the radial relative velocity at contact $\langle|w_r|\rangle$, the RDF $g(R)$ and the collision kernel all remain approximately constant or very slowly varying with $Re_T$. This observed difference between 2D and 3D is consistent with the anticipation by Onishi *et al.* (2013) that the intermittency may be the cause of the Reynolds number dependence of the collision statistics in 3D turbulence.

4.2.5. *Local flow statistics*

With the aim to get some insight into the effect of internal intermittency on the collision kernel, we investigate in this subsection the PDFs of $s^*(=\sqrt{2tr(\mathbf{s}^2)})$ (for both 3D and 2D) and $\epsilon^* = \nu s^{*2}$ (for 3D). Note that $St$ (the characteristic global Stokes number) can be written as $St = \tau_p/\tau_\eta = \tau_p\sqrt{2\langle tr(\mathbf{s}^2)\rangle}$.

The non-dimensional local flow strain rate, $\sigma^*$, is defined as

$$\sigma^* = \begin{cases} s^*\tau_\eta & \text{for 2D} \\ \sqrt{\epsilon^*/\epsilon} & \text{for 3D} \end{cases}, \tag{4.3}$$

where $\epsilon = \nu\langle s^{*2}\rangle$. This definition leads to $\int \sigma^{*2} PDF(\sigma^*)d\sigma^* = 1$ as $\langle s^{*2}\rangle \tau_\eta^2 = 1$. Figure 8 shows (a) the PDFs of the local flow strain rate, $\sigma^*$, and (b) the mean values of $\sigma^*$, $\langle\sigma^*\rangle$, against $Re_T$. Figure 8(a) shows that the most-likely $\sigma^*$, $\sigma^*_{likely}$, (where the PDF reaches

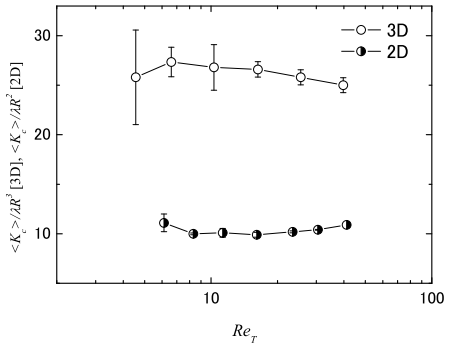


(a)

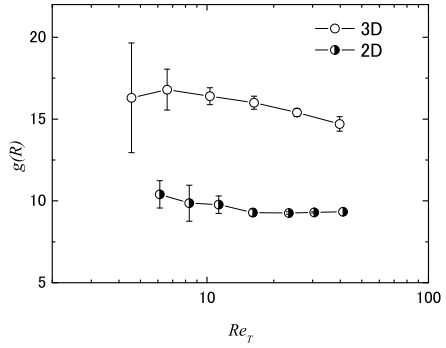


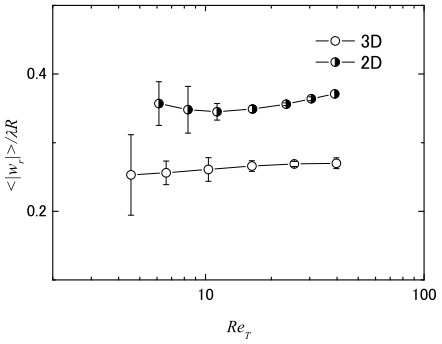


(b) (c)

FIGURE 7. (a) Collision kernel, (b) radial distribution function and (c) radial relative velocity at contact for $St$=0.4 plotted against $Re_T$.

its maximum) is smaller than unity and the probability of $\sigma^* > 3$ is negligibly small. The figure also shows that $\sigma^*_{likely}$ decreases with increasing $Re_T$ and that the decrease rate is larger in 3D than that in 2D. This trend is quantitatively mirrored in Figure 8(b), which shows that the 3D $\langle\sigma^*\rangle$ decreases with increasing $Re_T$ and that the 2D $\langle\sigma^*\rangle$ also decreases but at a smaller rate. This difference in the Reynolds number dependence is in line with the fact that the 3D flows have a stronger Reynolds number dependence of the flatness factor (see Figure 2).

The decrease of $\sigma^*_{likely}$ indicates that, as $Re_T$ increases, an increasing part of space is dominated by low local strain rates. Here let us define the *local* Stokes number, $St^*$, as $St^* = \sigma^* St$. Then the decreasing $\sigma^*_{likely}$ with increasing $Re_T$ is interpreted as a decreasing $St^*_{likely}$ (where the PDF reaches its maximum) as illustrated in Figure 9, where $St^*_{likely}$ is always smaller than unity since we limit the discussion for $St < 1$ in this study. The schematic illustration can explain, under the assumption that the clustering is strong for $St^* \sim 1$, the decreasing dependence of $g(R)$ on $Re_T$. As $Re_T$ increases, an increasing part of space is dominated by low local strain rates, i.e., small $St^*(<1)$, which would imply lower values of $g(R)$, while the extreme strain rates increase in increasingly small area of space. As the area of $St^* > 1$ cannot efficiently increase $g(R)$, the extreme strain rates cannot tip the balance and overcome the reduction in $g(R)$ caused by the reduced values

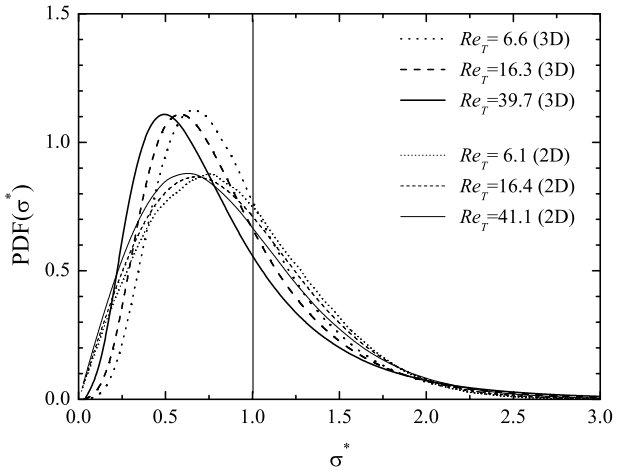


(a)

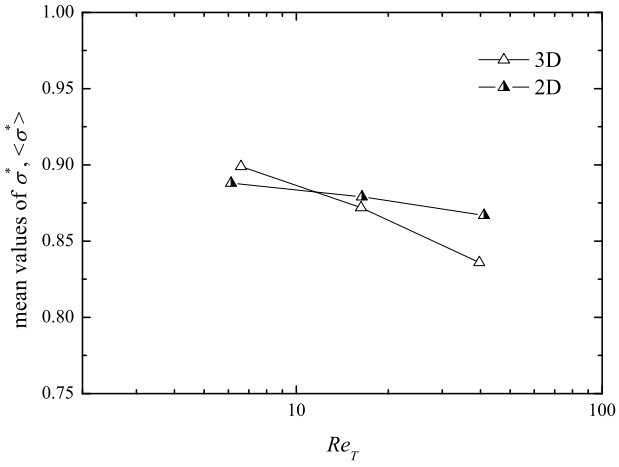


(b)

FIGURE 8. (a) Probability density functions and (b) mean values of the local strain rate, $\sigma^*$.

of local strain rates in most of the space. This mechanism for decreasing $g(R)$ could work as far as the extreme strain rates of $St^*$>1, i.e., $\sigma^* > 1/St$, hold some influence on the statistics. According to the PDFs in Figure 8(a), the probability of $\sigma^* > 3$ is negligibly small. Therefore, the mechanism would not work when $St \ll 1/3$, in which case the extreme strain rates may tip the balance and compensate the reduction in $g(R)$ caused by the reduced values of local strain rates in most of the space, making the $g(R)$ insensitive to the Reynolds number.

In order to support our argument on the Reynolds dependency of $g(R)$, we extend our discussion to two more Stokes numbers. Figure 10 shows $g(R)$ against $Re_T$ for three

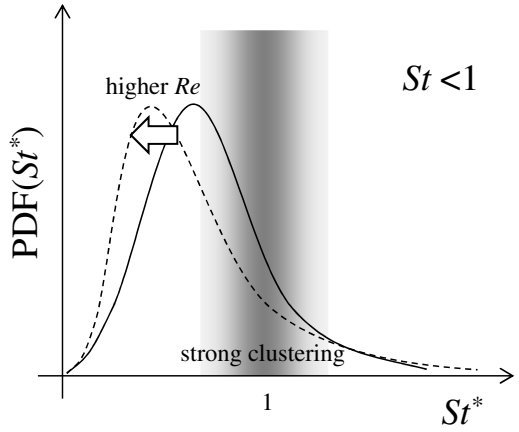


FIGURE 9. Schematic illustration of the mechanism of the decreasing clustering effect with higher Reynolds number with stronger intermittency.

different Stokes numbers; $St$=0.1, 0.4 and 0.6. The data for $St$=0.4 is the same as Figure 7(b), but the vertical axis is differently arranged. In Figures 10(b) and (c), the right axes is for 3D data and the left axes for 2D data. The ranges of right and left axes are in the same ratio, e.g., 9 to 21 for the right, while 6 to 14 for the left in Figure 10(b) in order to focus on the trend. The 3D DNS data for $St = 0.1$ and 0.6 have been obtained for the present study with almost the same numerical schemes and data processing for $St$=0.4 in Onishi *et al.* (2013). The sole difference from Onishi *et al.* (2013) is in the run duration for the smallest $Re_T$ (corresponds to the 3D simulation for $R_\lambda$=49 with $64^3$ grids and $32^3$ particles): each run duration for the smallest $Re_T$ for $St = 0.1$ and 0.6 was 4 times larger than the other 3D-DNS data in order to decrease the standard deviation.

Data for $St$=0.1 (i.e., $\ll 1/3$) are almost constant, or at least do not show any clear Reynolds number dependence, as predicted by our argument based on Figure 9. By contrast, for $St$=0.4 and 0.6, 2D and 3D data show variations against $Re_T$. The Reynolds number dependencies for small Reynolds number values are affected by the limited computational domain sizes. Here we focus on the Reynolds number dependence in the larger Reynolds number range where $Re_T$ is bigger than $Re_{T,crit}$ ($Re_{T,crit}$ differs in different data sets). For $St$=0.6, as in the case of $St$ =0.4, the 3D $g(R)$ decreases with Reynolds number range of $Re_T > Re_{T,crit}$, while the 2D $g(R)$ almost converges towards an approximately constant value. This further supports our argument illustrated in Figure 9. Note that $Re_{T,crit}$ has a dependence on $St$. For $St = 0.4$ is 7 and 16 for 3D and 2D, respectively, and for $St = 0.6$ it is 10 and 23 for 3D and 2D, respectively. That is, $Re_{T,crit}$ becomes larger for larger $St$. This may be caused by larger $St$ particles being influenced by larger flow motions with larger time scales, which would require larger domain sizes (i.e., larger $Re_T$) for this artificial effect to be eliminated. The present study limits the discussion to $St$<1, thus targeting the cloud droplets. A discussion of the Reynolds dependence of larger $St$ particles would require larger $Re_T$ data sets.

4.2.6. *Local particle statistics*

The non-dimensional local Stokes number of colliding pairs of particles can be defined as

$$\sigma_c^* = St_{col}^*/St, \tag{4.4}$$

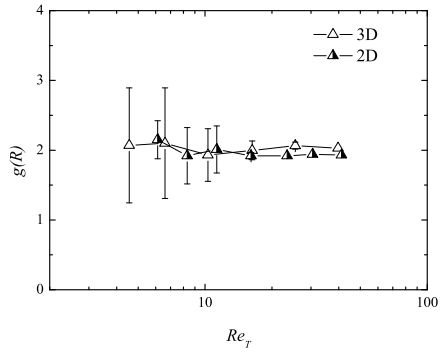


(a)$St$=0.1

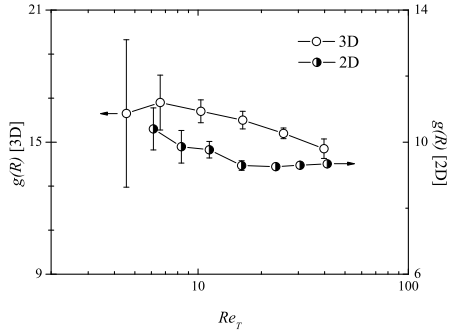


(b)$St$=0.4

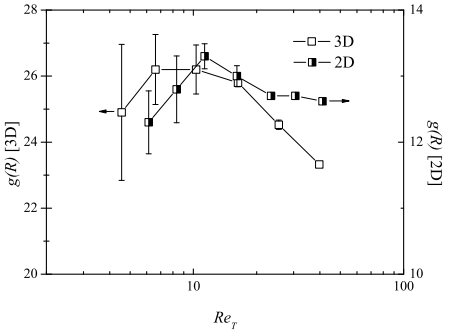


(c)$St$=0.6

FIGURE 10. Radial distribution function at contact, $g(R)$, plotted against $Re_T$ for (a) $St$=0.1, (b) $St$=0.4 and (c) $St$=0.6.

where $St^*_{col}$ is the local Stokes number at the location where the two particles collide. (Since all the particles have the same size in the system and the separation between the two colliding particles (i.e., $R$) is negligibly small compared to the grid size $\Delta$, we can safely assume that $St^*_{col}$ is the same for both particles. Therefore, only one of the two possible $St^*_{col}$ is processed.) Figure 11 shows the PDFs of $\sigma^*_c$. For both 3D and 2D, the right tails of the PDFs become thicker, i.e., the relative frequencies of strong events become larger with increasing $Re_T$. Interestingly, the $Re_T$-dependence of the tail thickness in 2D looks comparable with its counterpart in 3D. In order to quantify the $Re_T$-dependence of the relative frequency of strong events, we define the probability of strong events as

$$P(\sigma^*_c \geqslant 2) = \int_2^\infty PDF(\sigma^*_c) d\sigma^*_c. \tag{4.5}$$

Figure 12 shows $P(\sigma^*_c \geqslant 2)$ against $Re_T$. $P(\sigma^*_c \geqslant 2)$ in 2D depends on $Re_T$ and increases with increasing $Re_T$. This suggests that, even with little intermittency as is the case in 2D, the impact of rare but strong events increases with increasing $Re_T$. The argument by Dallas & Vassilicos (2011) that strong rare collision events enhance collision growth in high Reynolds number turbulence irrespective of internal intermittency (even if not supported for extremely small inertial particles in subsection 4.2.3) may nevertheless

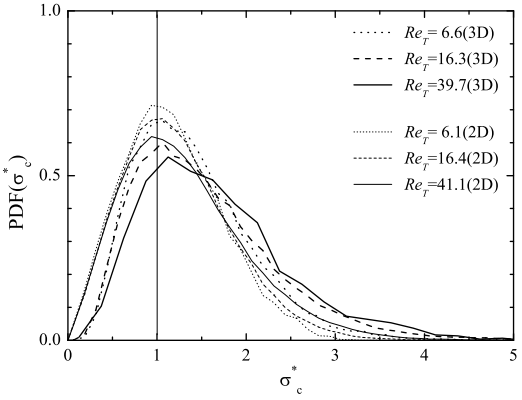


FIGURE 11. Probability density function of the non-dimensional local Stokes number of colliding pairs of particles, $\sigma_c^*$.

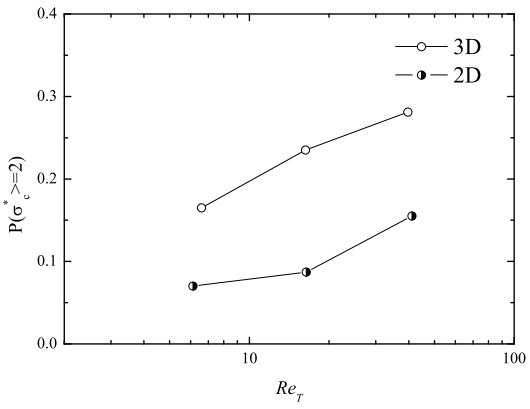


FIGURE 12. Probability for the case that $\sigma_c^*$ $(= St_{col}^*/St)$ exceeds 2.

be valid for non-negligibly small inertial particles. This mechanism which distinguishes between powerful rare collision events and internal intermittency requires a future study of its own based on new simulations run for larger values of $St$ and $Re_T$.

## 5. Conclusions

In this study, we have developed a direct numerical simulation (DNS) of colliding inertial particles in two-dimensional (2D) isotropic turbulence. The 2D DNS code is composed of the flow code by Goto & Vassilicos (2004), the particle code by Dallas & Vassilicos (2011) and the collision statistics code by Onishi *et al.* (2009). Using this combined code, we have investigated, for the first time, the detailed collision statistics in 2D isotropic turbulence. Firstly, the 2D version of the collision kernel model by Saffman & Turner (1956) for small Stokes particles, $St \ll 1$, has been formulated. It has then

been confirmed that the DNS results agree with the present 2D formulation. In turn, this confirmed the reliability of both the present 2D DNS code and the present formulation. Secondly, we have modified the spherical formulation for three-dimensional (3D) flows (Wang *et al.* 1998*b*) in order for it to be applicable in 2D. The Lagrangian pair radial relative velocity, $\langle|w_r|\rangle$, and the radial distribution function at contact, $g(R)$, depend on the thickness of the contact shell, $\delta$. We have observed a very similar dependence of $\langle|w_r|\rangle$ and $g(R)$ on $\delta$ in 2D as previously observed in 3D by Wang *et al.* (2000). As a result the value of $\delta$ was fixed at $\delta = 0.02R$, as in Wang *et al.* (2000), in this study. It has been confirmed that $g(R) - 1 \propto St^2$ and $\langle|w_r|\rangle / \lambda R = 1/2\sqrt{\pi}$ (=0.282) for $St \ll 1$ in the present 2D flow.

The 2D DNS results have been compared with the 3D DNS data of Onishi *et al.* (2013) for $St$=0.4 and with newly obtained 3D DNS data for $St$=0.1 and 0.6. Onishi *et al.* (2013) reported that, for $St = 0.4$, the collision kernel decreases with increasing Reynolds number, reflecting the decreasing trend of clustering effect. This study has investigated the role of turbulence intermittency in the Reynolds number dependency. The 3D turbulence has internal intermittency, while the 2D turbulence virtually none (Tabeling 2002). This has been confirmed in terms of the flatness factor $F = \left\langle (\partial u_1/\partial x_1)^4 \right\rangle / \left\langle (\partial u_1/\partial x_1)^2 \right\rangle^2$. We have observed that the clustering effect for the 3D flow decreases for $St = 0.6$ as well as for $St = 0.4$ in large Reynolds number ranges with increasing Reynolds number, while that for the 2D flow do not show a clear Reynolds number dependence in the corresponding large Reynolds number range. This observation supports the view that the Reynolds dependence of the clustering effect observed in 3D is due to internal intermittency of the 3D turbulence. We have further investigated the local flow strain rates ($\sigma^*$) and confirmed that an increasing part of space is dominated by low $\sigma^*$ as the Reynolds number increases, i.e., as the flow intermittency grows. This means that, as the Reynolds number increases, an increasing part of space is dominated by small $St^*$, where $St^*$ is the local Stokes number defined as $St^* = \sigma^* St$, which would decrease $g(R)$ when the most-likely $\sigma^*$ is smaller than unity. As the area of $St^* > 1$ cannot efficiently increase $g(R)$, the extreme strain rates cannot overcome the reduction in $g(R)$ caused by the reduced values of local strain rates in most of the space. This mechanism for decreasing $g(R)$ could work as far as the extreme strain rates of $St^*$>1, i.e., $\sigma^* > 1/St$, hold some influence on the statistics. The probability of $\sigma^* > 3$ is negligibly small. Therefore, the mechanism would not work when $St \ll 1/3$, in which case the extreme strain rates may compensate the reduction in $g(R)$ caused by the reduced values of local strain rates in most of the space, making the $g(R)$ insensitive to the Reynolds number.

A comparison between the 2D Lagrangian DNS and a stochastic simulation has revealed that the collision growth observed in Dallas & Vassilicos (2011) for initially $St = 0.04$ particles can be predicted by the conventional stochastic approach. However, for Stokes numbers not much smaller than unity (e.g., $St$=0.4), the PDF of local Stokes numbers sampled at the collision sites of particle pairs indicates that local strong collision events become increasingly frequent with increasing Reynolds number even in 2D inverse-cascading turbulence, i.e., irrespective of the internal intermittency of the turbulence.

## Acknowledgement

This research was conducted while Ryo Onishi was receiving a JSPS postdoctoral fellowship for research abroad. The large-size three-dimensional numerical simulations presented were carried out on the Earth Simulator 2 supercomputer in the Japan Agency

for Marine-Earth Science and Technology (JAMSTEC), while the two-dimensional simulations on the JAMSTEC supercomputer system. The 2D code developed in this study is based on the flow code provided by Dr. Susumu Goto and the particle code provided by Dr. Vassilios Dallas. The authors sincerely appreciate their kindness.

## REFERENCES

Abrahamson, J 1975 Collision rates of small particles in a vigorously turbulent fluid. *Chemical Engineering Science* **30** (11), 1371–1379.

Allen, M. P. & Tildesley, D. J. 1987 *Computer Simulation of Liquids*. Oxford University Press.

Ayala, O., Rosa, B. & Wang, L.-P. 2008 Effects of turbulence on the geometric collision rate of sedimenting droplets. part 2. theory and parameterization. *New J. Phys.* **10** (7), 075016.

Blyth, A. M. 1993 Entrainment in cumulus clouds. *J. Appl. Meteorol.* **32**, 626–641.

Bordas, R., Hagemeier, T., Wunderlich, B. & Thevenin, D. 2011 Droplet collisions and interaction with the turbulent flow within a two-phase wind tunnel. *Physics of Fluids* **23**, 085105.

Chen, L, Goto, S & Vassilicos, J. C 2006 Turbulent clustering of stagnation points and inertial particles. *J. Fluid Mech.* **553** (-1), 143.

Chun, J., Koch, D. L., Rani, S. L., Ahluwalia, A. & Collins, L. R. 2005 Clustering of aerosol particles in isotropic turbulence. *Journal of Fluid Mechanics* **536**, 219–251.

Coleman, S. W & Vassilicos, J. C 2009 A unified sweep-stick mechanism to explain particle clustering in two- and three-dimensional homogeneous, isotropic turbulence. *Phys. Fluids* **21** (11), 113301.

Dallas, V. & Vassilicos, J. C. 2011 Rapid growth of cloud droplets by turbulence. *Physical Review E* **84** (4), 1–5.

Derevyanko, S., Falkovich, G. & Turitsyn, S. 2008 Evolution of non-uniformly seeded warm clouds in idealized turbulent conditions. *New Journal of Physics* **10**, 075019.

Faber, T. & Vassilicos, J. C. 2010 Acceleration-based classification and evolution of fluid flow structures in two-dimensional turbulenc. *Physical Review E* **82**, 026312.

Falkovich, G. & Pumir, A. 2007 Sling effect in collisions of water droplets in turbulent clouds. *J. Atmos. Sci.* **64** (12), 4497–4505.

Franklin, C. N., Vaillancourt, P. A. & Yau, M. K. 2007 Statistics and parameterizations of the effect of turbulence on the geometric collision kernel of cloud droplets. *Journal of the Atmospheric Sciences* **64** (3), 938–954.

Goto, S., Osborne, D.R., Vassilicos, J.C. & Haigh, J.D. 2005 Acceleration statistics as measures of statistical persistence of streamlines in isotropic turbulence. *Physical Review E* **71**, 015301(R).

Goto, S. & Vassilicos, J.C. 2004 Particle pair diffusion and persistent streamline topology in two-dimensional turbulence. *New J. Phys.* **6**, 65.

Grabowski, W. W. & Wang, L.-P. 2009 Diffusional and accretional growth of water drops in a rising adiabatic parcel: effects of the turbulent collision kernel. *Atmos. Chem. Phys* **9**, 2335–2353.

Grabowski, W. W. & Wang, L.-P. 2013 Growth of cloud droplets in a turbulent environment. *Annu. Rev. Fluid Mech.* **45**, 293–324.

Krueger, S. K., Su, C. W. & McMurtry, P. A. 1997 Modeling entrainment and finescale mixing in cumulus clouds. *J. Atmos. Sci.* **54** (23), 2697–2712.

Lu, J., Nordsiek, H., Saw, E. W. & Shaw, R. A. 2010 Clustering of charged inertial particles in turbulence. *Phys. Rev. Lett.* **104** (18), 184505.

MacPherson, J. I. & Isaac, G. A. 1977 Turbulent characteristics of some canadian cumulus clouds. *Journal of the Applied Meteorology* **16**, 81–90.

Maxey, M. R. 1987 The gravitational settling of aerosol particles in homogeneous turbulence and random flow fields. *Journal of Fluid Mechanics* **174**, 441–465.

Onishi, R. 2005 Numerical simulations of chemical reaction and droplet growth in environmental turbulent flows. PhD thesis, Kyoto University.

Onishi, R., Takagi, H., Takahashi, K. & Komori, S. 2006 Turbulence effects on cloud droplet collisions in mesoscale convective clouds. *Turbulence, Heat and Mass Transfer* **5**, 709–712.

Onishi, R., Takahashi, K. & Komori, S. 2009 Influence of gravity on collisions of monodispersed droplets in homogeneous isotropic turbulence. *Physics of Fluids* **21**, 125108.

Onishi, R., Takahashi, K. & Komori, S. 2011 High-resolution simulations for turbulent clouds developing over the ocean. *Gas Transfer at Water Surfaces 2010* **6**, 582–592.

Onishi, R., Takahashi, K. & Vassilicos, J. C. 2013 An efficient parallel simulation of interacting inertial particles in homogeneous isotropic turbulence. *Journal of Computational Physics* **242**, 809–827.

Rosa, B., Parishani, H., Ayala, O., Grabowski, W. & L.-P., Wang 2013 Kinematic and dynamic collision statistics of cloud droplets from high-resolution simulations. *New Journal of Physics* .

Saffman, P. G. & Turner, J. S. 1956 On the collision of drops in turbulent clouds. *Journal of Fluid Mechanics* **1** (01), 16–30.

Saw, E. W., Shaw, R. A., Ayyalasomayajula, S., Chuang, P. Y. & Gylfason, A. 2008 Inertial clustering of particles in high-reynolds-number turbulence. *Phys. Rev. Lett.* **100** (21), 214501.

Sidin, R. S. R., Ijzermans, R. H. A. & Reeks, M. W. 2009 A lagrangian approach to droplet condensation in atmospheric clouds. *Phys. Fluids* **21** (10), 106603.

Siebert, H., Lehmann, K. & Wendisch, M. 2006 Observations of small-scale turbulence and energy dissipation rates in the cloudy boundary layer. *Journal of the Atmospheric Sciences* **63**, 1451–1466.

Sundaram, S. & Collins, L.R. 1996 Numerical considerations in simulating a turbulent suspension of finite-volume particles. *Journal of Computational Physics* **124** (2), 337–350.

Sundaram, S. & Collins, L. R. 1997 Collision statistics in an isotropic particle-laden turbulent suspension. part 1. direct numerical simulations. *Journal of Fluid Mechanics* **335**, 75–109.

Tabeling, P. 2002 Two-dimensional turbulence: a physicist approach. *Physics Reports* **362**, 1–62.

Taylor, G. I. 1935 Statistical theory of turbulence. *Proceedings of the Royal Society of London. Series A* **151**, 421–444.

Van Den Heever, S. C. & Cotton, W. R. 2007 Urban aerosol impacts on downwind convective storms. *J. Appl. Meteor. Climatol.* **46** (6), 828–850.

Wang, L.-P., Rosa, B., Gao, H., He, G. & Jin, G. 2009 Turbulent collision of inertial particles: Point-particle based, hybrid simulations and beyond. *International Journal of Multiphase Flow* **35** (9), 854–867.

Wang, L.-P., Wexler, A. S. & Zhou, Y. 1998*a* On the collision rate of small particles in isotropic turbulence. i. zero-inertia case. *Physics of Fluids* **10**, 266–276.

Wang, L.-P., Wexler, A. S. & Zhou, Y 1998*b* Statistical mechanical descriptions of turbulent coagulation. *Physics of Fluids* **10**, 2647–2651.

Wang, L.-P., Wexler, A. S. & Zhou, Y. 2000 Statistical mechanical description and modelling of turbulent collision of inertial particles. *J. Fluid Mech.* **415**, 117–153.

Xue, Y., Wang, L.-P. & Grabowski, W.W. 2008 Growth of cloud droplets by turbulent collision–coalescence. *J. Atmos. Sci.* **65** (2), 331–356.

Yin, Y., Levin, Z., Reisin, T. G. & Tzivion, S. 2000 The effects of giant cloud condensation nuclei on the development of precipitation in convective clouds – a numerical study. *Atmospheric Research* **53** (1-3), 91 – 116.

Yoshimatsu, K., Okamoto, N., Schneider, K., Kaneda, Y. & Farge, M. 2009 Intermittency and scale-dependent statistics in fully developed turbulence. *Phys. Rev. E* **79** (2), 026303.

Zaichik, L. & Alipchenkov, V. 2009 Statistical models for predicting pair dispersion and particle clustering in isotropic turbulence and their applications. *New J. Phys.* **11**, 3018.

Zaichik, L., Simonin, O. & Alipchenkov, V. 2003 Two statistical models for predicting collision rates of inertial particles in homogeneous isotropic turbulence. *Physics of Fluids* **15**, 2995–3005.

Zhou, Y., Wexler, A. S. & Wang, L.-P. 2001 Modelling turbulent collision of bidisperse inertial particles. *J. Fluid Mech.* **433**, 77.